

**Laser-induced cavitation in acoustically  
levitated droplets**

Internship at the Cavitation Lab,  
Nanyang Technological University,  
Singapore.

11.04.2015-19.06.2015

Pjotr Kerssens (s1005766)

**UNIVERSITY OF TWENTE.**

# MSc Internship report

Pjotr Kerssens, s1005766

## **Institution details**

*Cavitation Lab*

*Division of Physics and Applied Physics*

*School of Physical and Mathematical Sciences*

*Nanyang Technological University*

*21 Nanyang Link*

*637371 Singapore*

**Mentor:** Assoc Prof Claus-Dieter Ohl

**Supervisor:** Dr Silvestre Roberto Gonzalez-Avila

**Internship period:** 11.04.2015 - 19.06.2015

# Abstract

In this internship, the behaviour of laser-induced cavitation bubbles in acoustically levitated water droplets has been investigated. Because such a bubble is confined in a small volume of liquid, a lot of interactions occur. Firstly, the bubble interacts with the droplet surface, creating fast jets emitted from the droplet surface. If the laser carries sufficient energy, the cavitation bubble can even rupture the droplet surface and create a liquid sheet, or even atomize the entire droplet. Secondly, shockwaves are emitted when the bubble is created and every time that the bubble collapses. These shockwaves also interact with the droplet, leading to capillary waves on the droplet surface, emission of jets from the droplet surface and the creation of short-lived secondary cavitation bubbles inside the water droplet. All of these phenomena have been captured with a high-speed camera during this internship, providing valuable insight into the physics governing this phenomenon. Additionally, 3D videos of the same phenomena have been recorded as well using a stereoscopic high-speed camera configuration. Lastly, the existing acoustic levitation setup has been improved to provide better levitation at lower input voltages.

***Keywords:***

*laser-induced cavitation, acoustic levitation, bubble surface interaction, Richtmyer Meshkov instability, high speed imaging, stereoscopy*

# Preface

In the Mechanical Engineering Master's programme at the University of Twente, all students have to perform an internship within a company, university or research institute to learn to put knowledge into practice and to get a feeling for the type of careers that are possible for mechanical engineers. For a lot of students, it is also a chance to go abroad, and for me that was no different. Because I also wanted to learn how to work with people from backgrounds that are very different from the Dutch culture, I chose to do an internship at the Nanyang Technological University (NTU) in Singapore, from 11 April to 19 June 2015, which is a period of in total ten weeks. This university is highly acclaimed worldwide, which was also a learning for me: what is it like to work at a modern yet prestigious university?

At the NTU I was a research intern within the Cavitation Lab led by professor Claus-Dieter Ohl, a specialist on the area of cavitation. My direct supervisor was Silvestre Roberto Gonzalez Avila, who at the time was working on laser-induced cavitation in acoustically levitated droplets. As research intern I assisted him in his experiments, mainly by performing experiments on larger droplets, which had until then not been investigated, and by adjusting the setup to enable alternative experiments. This involved a lot of freedom, which taught me to set my own priorities and discover my own interests.

Many people are to thank for this internship. First and foremost I would like to thank professor Harry Hoeijmakers from the Engineering Fluid Dynamics department at the University of Twente, who was my university supervisor. He established contact between me and the Cavitation Lab at the NTU in Singapore, thus enabling this very valuable professional experience. Naturally, I would also like to thank all group members of the Cavitation Lab for guiding me during my research. In particular I would like to thank Roberto for his supervision, Claus-Dieter for his input and the administrative and financial support granted, and Julien Rapet for being an outstanding sounding board.

*Pjotr Kerssens*

# Contents

<b>1</b>	<b>Introduction</b>	<b>1</b>
<b>2</b>	<b>Theoretical background</b>	<b>2</b>
2.1	Cavitation bubble behaviour . . . . .	2
2.1.1	Bubble-surface interaction . . . . .	2
2.2	Influence of the shockwave . . . . .	3
2.2.1	Richtmyer-Meshkov instability . . . . .	3
2.2.2	Secondary cavitation . . . . .	5
2.3	Acoustic levitation . . . . .	6
2.3.1	Influence of geometry . . . . .	6
2.4	Stereoscopic imaging . . . . .	7
2.5	Conclusion . . . . .	9
<b>3</b>	<b>Experimental setup &amp; methods</b>	<b>10</b>
3.1	Setup . . . . .	10
3.1.1	Acoustic levitator . . . . .	10
3.1.2	Laser setup . . . . .	10
3.1.3	Camera setup . . . . .	11
3.2	Methods . . . . .	12
3.2.1	Normal images processing . . . . .	12
3.2.2	Stereoscopic images processing . . . . .	13
3.3	Conclusion . . . . .	13
<b>4</b>	<b>Results</b>	<b>14</b>
4.1	Bubble-surface interaction . . . . .	14
4.2	Shockwave influence . . . . .	14
4.2.1	Richtmyer-Meshkov instability . . . . .	15
4.2.2	Secondary cavitation . . . . .	16
4.3	Acoustic levitation . . . . .	16
4.4	Stereoscopic images . . . . .	19
<b>5</b>	<b>Conclusions</b>	<b>21</b>
<b>A</b>	<b>Calibration procedure</b>	<b>22</b>
A.1	MATLAB code . . . . .	22
<b>B</b>	<b>Anaglyph movie code</b>	<b>28</b>
B.1	MATLAB code . . . . .	28

# 1 Introduction

Cavitation in small droplets is a subject studied by a number of research groups for various reasons: because it provides a means to create liquid tin sheets for the creation of XUV light [1] [2], because it allows for investigation of the dynamics of cavitation bubbles near surfaces, which is of relevance for most applications of cavitation [3], or because of interest in the fundamental properties of the phenomenon [4].

The interaction of a cavitation bubble and the cavitation-induced shock waves with the droplet surface of an acoustically levitated droplet is relevant for all of those fields of interest. Therefore the work conducted during this research is focused on this, though the methods of levitation and visualisation have been investigated too. The research question to be answered is:

*What is the influence of a laser-induced cavitation bubble and the shock waves caused by this bubble on an acoustically levitated, millimetre-sized water droplet?*

Three factors limit the study of the bubble-droplet interaction: the time scale on which the interactions occur, the size of the geometries studied and the timing irreproducibility of the process. To work around these limitations, this research focused mainly on the dynamics of droplets ranging from 1 to 3 mm. For droplets of that size, the processes involved are slower, the bubbles can be larger, and features are more pronounced.

In this report the results from my research are presented. I will start with the theoretical background on cavitation, the interaction between the bubble and the droplet surface and the interaction between shockwaves and the droplet surface, acoustic levitation and high-speed and stereo imaging. Next I will give a detailed description of the experimental set-up, and then I will present the results of my studies. I will end with some conclusions and recommendations.

## 2 Theoretical background

In this chapter, the theoretical background needed to understand the setup, the methods and the experiments of this research are presented. This is done stepwise: the first two sections deal with theoretical topics concerning cavitation and shockwaves, and the latter two introduce acoustic levitation and stereoscopic imaging techniques, respectively.

### 2.1 Cavitation bubble behaviour

Research into the phenomenon of cavitation is well-established, as it already started early in the twentieth century with Lord Rayleigh's research into the collapse of spherical cavities [5]. He was the first to describe the development of the radius of a spherical bubble in an infinite body of liquid with an elementary version of what is now known as the Rayleigh-Plesset equation [6].

A cavitation bubble is an unstable vapour bubble immersed in a liquid. The formation of such a bubble can start for different reasons. In the classical case, the bubble is formed by pressure differences in the liquid: as soon as the pressure locally drops below the vapour pressure, liquid will vaporise and form a vapour bubble. With interest in cavitation sparked by the maritime industry, where ship propellers produce cavitation bubbles, it is no wonder that these bubbles were discovered first [7]. Later, as research continued, other ways of creation of the cavity, such as laser-induced cavitation, were discovered. [7]. This technique is also used in this research. However, the method of bubble creation does not matter for the dynamics of the bubble. As soon as the bubble has reached a uniform composition, its dynamics can always be described by the Rayleigh-Plesset equation [8]:

$$\frac{P_B - P_\infty(t)}{\rho_L} = R_b \frac{d^2 R_b}{dt^2} + \frac{3}{2} \left( \frac{dR_b}{dt} \right)^2 + \frac{4\nu_L}{R_b} \frac{dR_b}{dt} + \frac{2S}{\rho_L R_b} \quad (2.1)$$

In the above formula, a viscosity term has been added with respect to the original formula derived by Plesset [6].

A cavitation bubble is inherently unstable: due to internal thermodynamic changes the bubble will grow and shrink and eventually disappear. An example of this bubble behaviour can be seen in fig. 2.1. It is known that this process causes a shockwave every time that the bubble collapses. Bubbles that are created forcibly, like our laser-induced bubble, also emit a shockwave when created by the laser [3]. The strength of the emitted wave gets lower with every collapse [7]. Both the cavitation bubble itself and the emitted shockwaves have a profound effect on the bubble that hosts them, as will be outlined in the next sections.

#### 2.1.1 Bubble-surface interaction

Close to a free surface the spherical symmetry assumed in the Rayleigh-Plesset equation does not hold anymore, so that the bubble will not show symmetrical behaviour in this case. This causes some interesting interactions with the free surface.

As explained by Robinson, Blake, Kodama, Shima and Tomita [9], the free surface is a zero-inertia limit. The bubble will therefore push the liquid towards the free surface during its expansion, causing a pressure peak in between the surface and the bubble. When the bubble is close enough, the pressure peak can form a spike on the free surface. Next, when the cavitation bubble starts to collapse, more fluid flows into the region between the free surface and the bubble, increasing the pressure there. As a result, another liquid

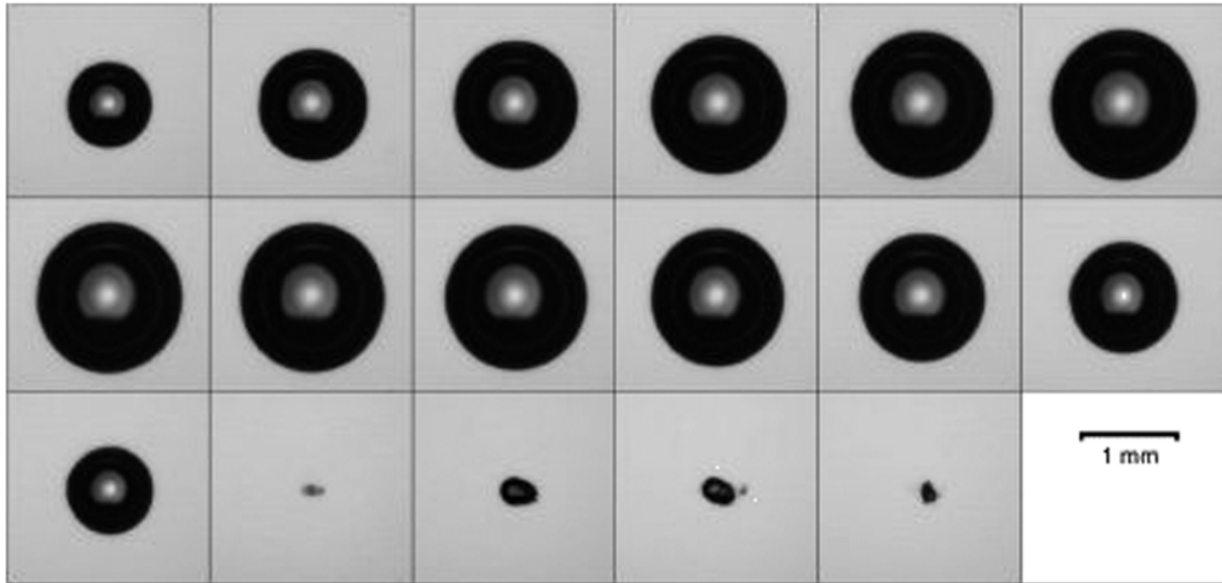


**Figure 2.1:** *Photographic series of the oscillation of a laser induced bubble. Starting time:  $10\ \mu\text{s}$  after bubble generation. Interframe time:  $10\ \mu\text{s}$ . Source: [7]*

jet is created that moves away from the free surface and pierces the cavitation bubble. This counterjet eventually ruptures the bubble, leaving a torus. This torus is then pushed downward by the counterjet, away from the free surface [9]. Both jets can clearly be seen in fig. 2.2, which shows an image sequence for such a bubble.

Bubble-surface interaction plays a role for cavitation inside a droplet as well, but the behaviour is slightly different. This has been extensively covered in a paper by Obreshkow et al. [3]. A splash erupting from the free surface is observed in this situation too, but the splash now is much broader. According to Obreshkow et al. this is because the distance between droplet and bubble varies more smoothly, leading to a broader pressure peak. The microjet that pierces the cavitation bubble can also be seen again, and has so much momentum that it actually escapes from the droplet on the side opposite to where the bubble was created. Both phenomena can be seen in fig. 2.3.

## 2.2 Influence of the shockwave

As mentioned in section 2.1, the cavitation bubble will create a shockwave when it is created and when it collapses. These shockwaves have just as big an impact on the droplet as the cavitation bubble itself, and are even potentially capable of breaking up the droplet. The shockwave itself, though it can be heard by the human ear and recorded with a hydrophone, is hard to register visually because it travels at supersonic speeds. However, the effects that the shockwave has on the droplet become visible in some cases, as the shockwave carries a lot of energy. Two such phenomena caused by the shockwave are considered in this report, and will therefore be explained. They are the Richtmyer-Meshkov instability, and shock-induced, or secondary, cavitation.

### 2.2.1 Richtmyer-Meshkov instability

In 1960, Robert D. Richtmyer extended the model for the Rayleigh-Taylor instability, which describes fluid interfaces that are continuously accelerated, with a model for a shock-accelerated fluid interface [10]. His work was later verified experimentally by E.E. Meshkov [11], and the instability of a shock accelerated fluid interface is therefore presently known as the Richtmyer-Meshkov instability.

In the basic, incompressible, linear version of the Richtmyer-Meshkov instability, a 2D geometry is considered with an initial perturbation  $\eta$  on the interface between the two fluids. This perturbation starts

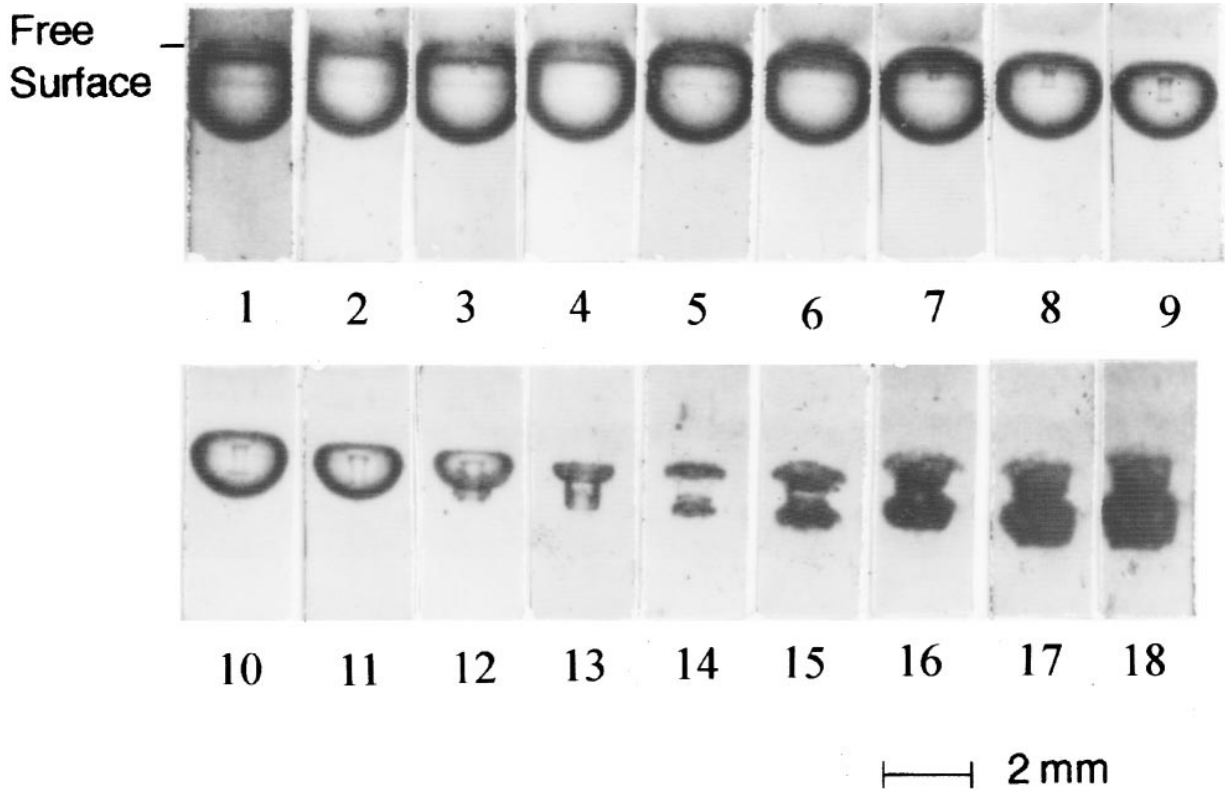


**Figure 2.2:** *Liquid jet development for a cavitation bubble created close to a free surface. Frame interval: 10  $\mu$ s. Source: [9]*

to grow as soon as a normal shock, travelling through fluid 1, hits the interface and is partially reflected and partially transmitted transmitted to fluid two. Modelling the shockwave as an impulsive acceleration, the resulting rate of growth of the perturbation is given by [12]:

$$\dot{\eta}_{imp} = k[u]A\eta_0 \quad (2.2)$$

with  $k$  the wave number,  $[u]$  the (instantaneous) change in velocity,  $A$  the Atwood number  $(\rho_A - \rho_L)/(\rho_L + \rho_A)$  and  $\eta_0$  the amplitude of the initial surface perturbation. This means that the growth of the perturbation is linear in time. When considering a shock travelling from a lighter to a heavier fluid, which is the base case considered in a lot of papers, the evolution of the instability roughly looks like in fig. 2.4.

### In water droplets

Most research for the Richtmyer-Meshkov instability focuses on gas-gas interfaces, as experimental results for this case can be obtained in a shock tube. This means that in most papers, surface tension is neglected. Also, most papers focus on a non-curved interface which has a small, harmonic perturbation and is accelerated by a shock travelling from the lighter to the heavier fluid.

This situation differs from the situation encountered for a liquid droplet with an internally generated shockwave. The differences between those situations, that have already been described in several papers, will be outlined next.

Firstly, the perturbation undergoes phase inversion if the shockwave travels from the heavy to the light fluid: the spikes of liquid penetrating into the gas turn into bubbles of gas penetrating into the liquid, and vice versa [13]. This can actually already be deduced from eq. (2.2): because the Atwood number is negative in this case, the change in amplitude will be negative as well, implying phase inversion.

Secondly, the presence of surface tension has a profound effect on the behaviour of the interface. As shown by Karnig O. Mikaelian [14], the surface tension will stabilize the system, so that the surface perturbations will oscillate rather than grow. The dispersion relation for these oscillations, as derived by Mikaelian, is:

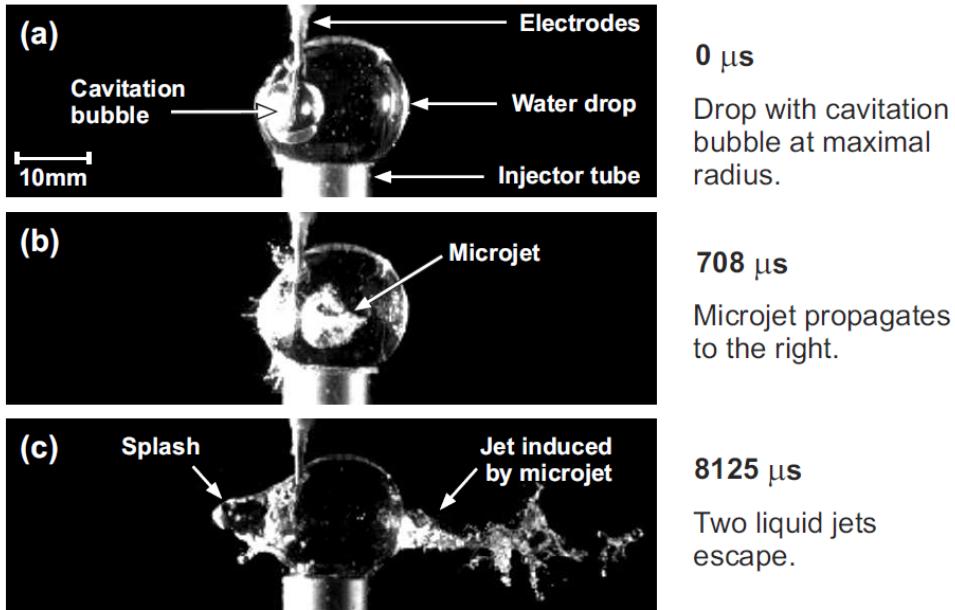


Figure 2.3: Cavitation bubble inside of a water droplet. Source: [3]

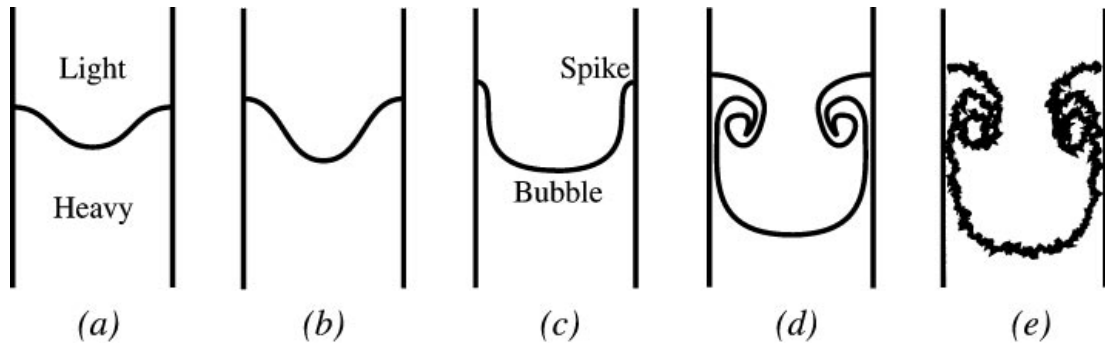


Figure 2.4: The development of the Richtmyer-Meshkov instability on a light-heavy fluid interface. Source: [12]

$$\omega = \sqrt{\frac{k^3 S}{\rho_A + \rho_L}} \quad (2.3)$$

This is the dispersion relation for capillary waves, and therefore ripples should theoretically occur on a surface with surface tension accelerated by a shock. The oscillatory movement of those ripples is described by:

$$\frac{\eta}{\eta_0} = \cos(\omega t) + \frac{[u]kA}{\omega} \sin(\omega t) \quad (2.4)$$

However, this equation is a result of linear theory and neglects the influence of viscosity. Experimental results therefore might differ from this model.

## 2.2.2 Secondary cavitation

Not only the bubble surface is affected by interaction with a shockwave, but the internal fluid as well. Here it can lead to a phenomenon called secondary cavitation: tiny gas bubbles in the fluid excited by the shockwave grow to visible size and collapse again shortly after that, creating a short-lived bubble “mist”.

Possible causes for the presence of these bubbles include evaporation of liquid on the convergent path of the laser [7] and the presence of growth nuclei such as impurities and dissolved gas [3]. Under favourable circumstances, this secondary cavitation can become visible. Such circumstances could be a reduced static pressure [7] or shockwave confinement due to the bubble geometry [3]. An example can be seen in fig. 2.5. Because the droplets used in the experiments in this research also allow for multiple shockwave reflections, it is expected that secondary cavitation will occur here as well.

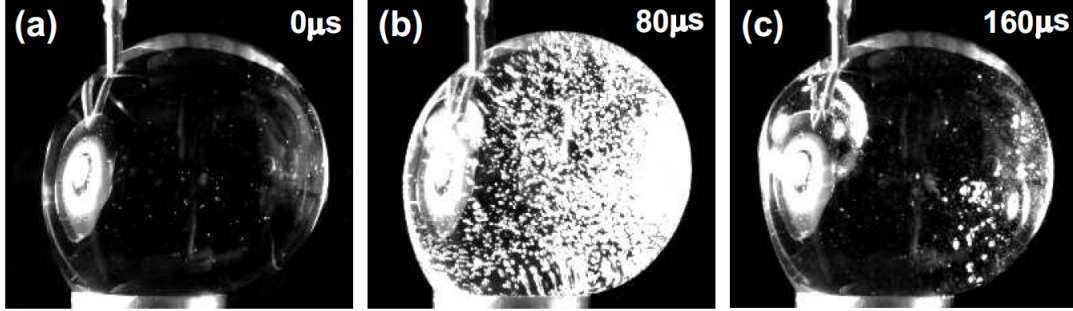


**Figure 2.5:** *Example of secondary cavitation. The shockwave created at the initiation of bubble growth causes a short-lived bubble mist, as can be seen in picture (b). Source: [3]*

## 2.3 Acoustic levitation

The research undertaken for this report makes use of acoustic levitation, a recently developed technique that makes use of ultrasonic waves to make objects hover. A (simple) acoustic levitator consists of an ultrasonic transducer and reflector. The transducer generates a standing wave between the transducer and the reflector, and that standing wave creates a force on any particle that is in its field. The force can be determined using the radiation potential  $U$ , which is described by [15]:

$$U = 2\pi R_d^3 \left( \frac{\overline{p^2}}{3\rho_A c^2} - \frac{\overline{\rho_A u^2}}{2} \right) \quad (2.5)$$

This formula is valid for spherical objects. The force acting on the sphere is then given by

$$F = -\nabla U \quad (2.6)$$

This means that all pressure antinodes (i.e. all minima of the radiation potential) are stable positions for acoustic levitation.

### 2.3.1 Influence of geometry

The geometry of the levitation setup has a strong influence on the radiation potential. Two factors can be distinguished here: the distance between the transducer and the reflector, and the shape of the reflector. The distance between the transducer and the reflector is so important, because a standing wave needs to be created for acoustic levitation to occur. This automatically means that the distance between the transducer has to be (approximately) a multiple of half a wavelength. As can be seen in fig. 2.6, the intensity of the potential field decreases for increasing distance. The reflector and transducer should therefore preferably be half a wavelength away from each other.

On the other hand, the shape of the reflector is important, because a flat reflector actually does a rather poor job at reflecting the incoming wave back to the transducer. A lot of energy thus gets lost when using a flat reflector. Therefore, a lot of authors actually use a curved reflector, because this allegedly increases the acoustic radiation force by focussing the reflection in the direction of the incoming wave [15]. Comparing fig. 2.7 (b) and fig. 2.6 (d), which show numerical simulations of the acoustic radiation field performed by Andrade et al., indeed leads to that conclusion: with the same driving signal, the curved

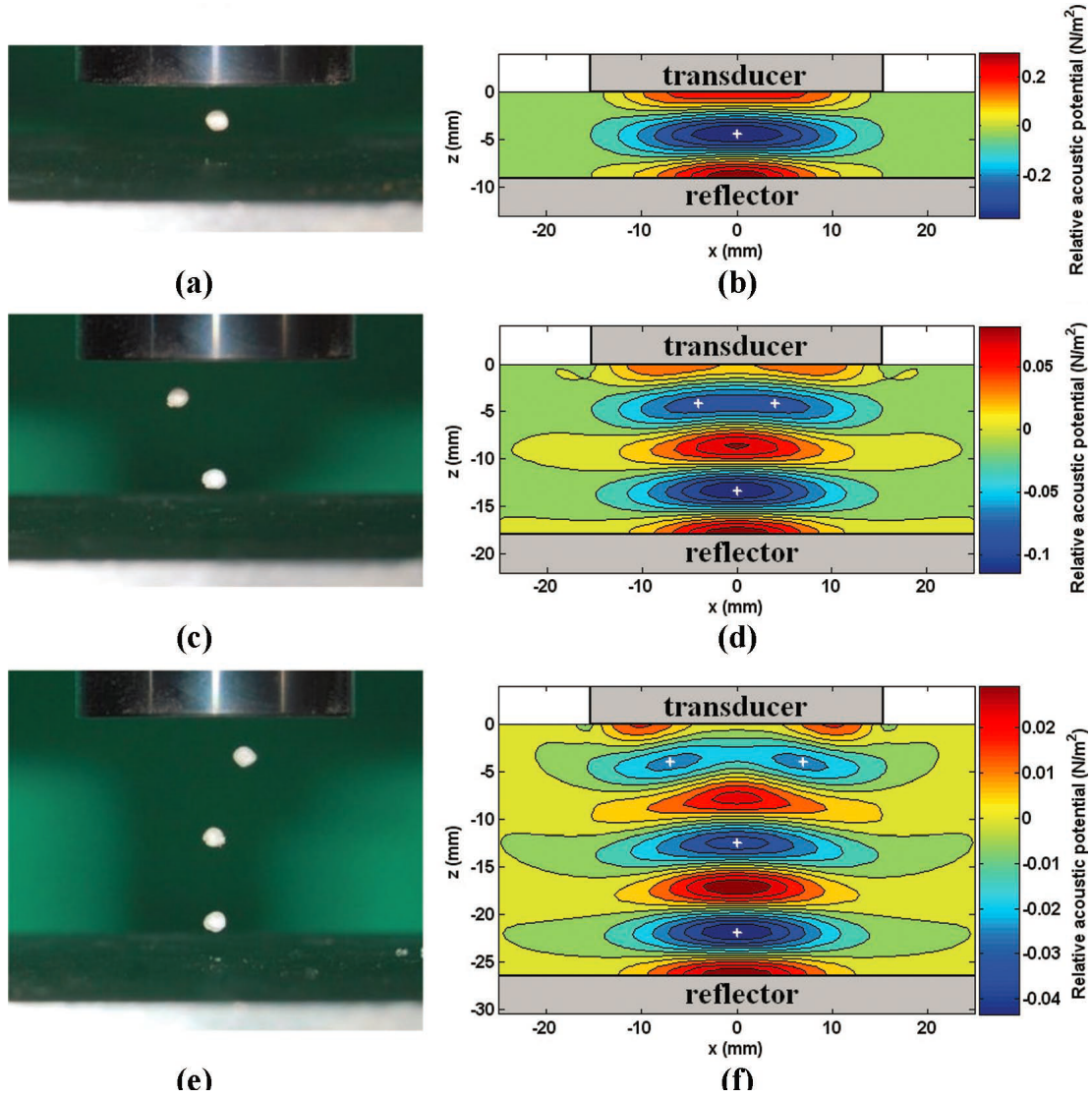


**Figure 2.6:** Acoustic radiation potential for different distances between transducer and reflector: 9 mm (a and b), 18 mm (c and d) and 26.5 mm (e and f). The relative acoustic potential, normalized by  $2\pi R^3$ , has been plotted here. Source: [15]

reflector gives a stronger acoustic potential field and an increased acoustic radiation force [15].

## 2.4 Stereoscopic imaging

Stereoscopic imaging is a technique that has boomed in recent years, not only with the arrival of 3D film in popular culture, but also with the arrival of 3D measuring techniques in, among others, physics of fluids. The basic principle is simple: two pictures of the same object made by two shifted cameras will show two slightly different scenes. From the differences between those two pictures, information about movements out of plane can be derived.

When this is done to measure positions, velocities and accelerations, care has to be taken that both camera's have the exact same object plane, with the same depth of field, so that objects have the same magnification in both image planes. This is usually done by applying the Scheimpflug condition to the configuration, i.e. by tilting the image and lens planes with respect to the object plane [16]. However, in this research, stereoscopic imaging is used for visualization rather than for measurements. Therefore it is not necessary to apply the Scheimpflug condition, and normal cameras can be used.

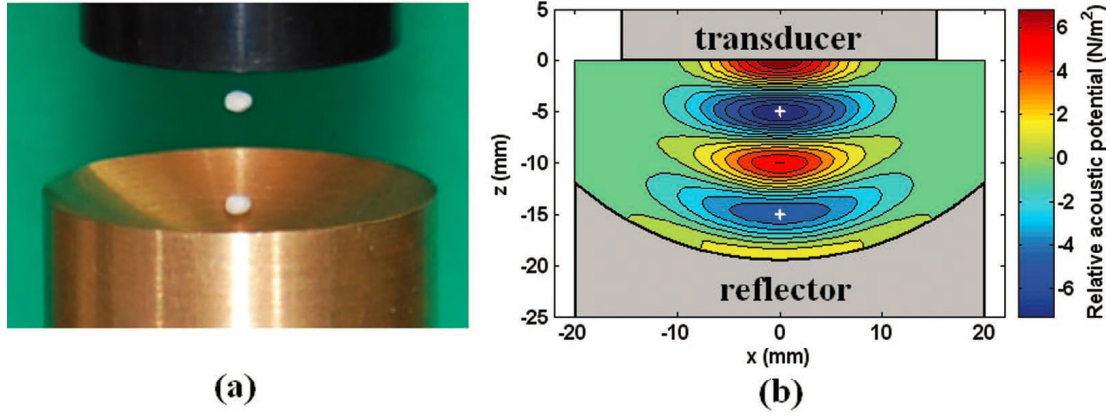


**Figure 2.7:** Acoustic radiation potential for a spherical reflector. As in fig. 2.6, the relative acoustic potential is plotted. Source: [15]

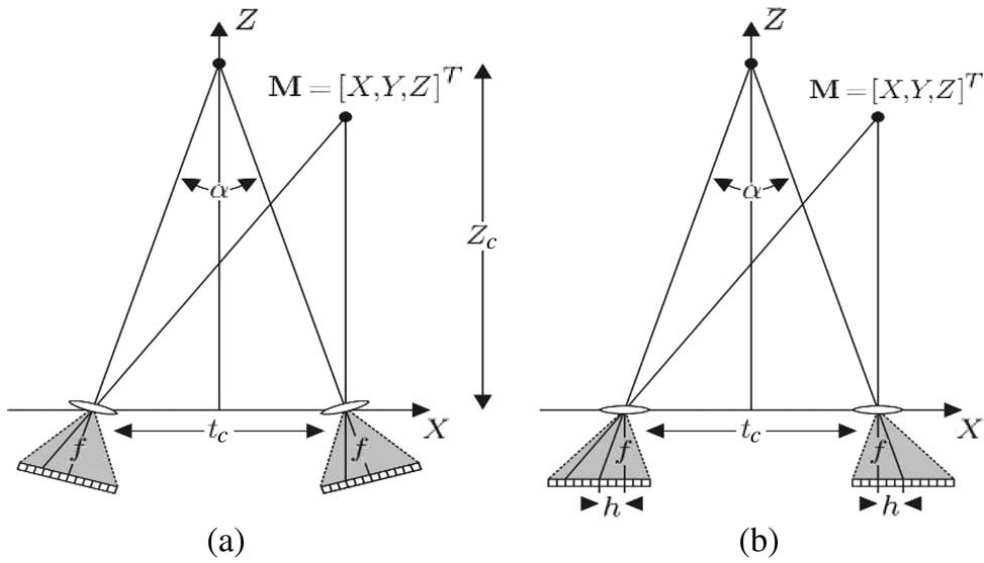


**Figure 2.8:** The possible configurations for stereoscopic imaging: (a) toed-in; (b) parallel. Source: [17]

With those “normal” cameras, where the angle between lens and film cannot be changed, two basic configurations can be used to shoot 3D footage: a toed-in and a parallel setup [17]. Both configurations are shown in fig. 2.8 In the toed-in configuration, both cameras are set a distance  $t_c$  apart and they are both tilted inward with the same angle so that they converge at some point (fig. 2.8 (a)). In the parallel setup, the cameras are pointing in the same direction. Then, either both pictures have to be cropped to leave only the overlapping region (not shown), or the sensors are shifted with respect to the lens to create overlapping object planes (fig. 2.8 (b)).

Of these two configurations, the parallel setup provides an undistorted image, but the toed-in setup is slightly easier to implement. Therefore, the toed-in configuration will be used in this research.

Some basic rules, based on human anatomy, should be applied to the configuration to create natural pictures. The most important rule is the 1/30 rule: the distance between the two cameras (the baseline,  $t_c$  in fig. 2.8) should be approximately 1/30th of the object distance ( $Z_c$  in fig. 2.8) [17]. This is because the human eyes can only focus on objects that are reasonably far away. As the average distance between the human eyes is 65 mm, a configuration that satisfies the 1/30 rule puts an object at a perceived distance of about 2 m from the viewer, which is a comfortable distance for the human eyes. The baseline can be widened or shortened to respectively increase or decrease the perception of depth, and this trick is used extensively in stereoscopic imaging.

Normally, attention has to be paid to the maximum depth of field as well. However, the high speed imaging used for this research needs a lot of illumination and therefore a big aperture. This automatically leads to a shallow depth of field, so that the accommodation-convergence issues that normally haunt stereoscopic imaging are already avoided in this case.

## **2.5 Conclusion**

This chapter has presented some phenomena that should occur when a cavitation bubble is created inside of a droplet. It also has presented some background on techniques that are used during this research, namely acoustic levitation and stereoscopic imaging. This background will come in handy for the next chapter, that describes the setups and methods used during this research.

## 3 Experimental setup & methods

During the internship, I performed experiments to investigate cavitation in acoustically levitated droplets. The details of the setup and methods used in those experiments are discussed in this chapter.

### 3.1 Setup

In the experiments for this research, laser-induced cavitation in acoustically levitated droplets is investigated. A schematic layout of the setup can be found in fig. 3.1. The different components of the setup are:

1. An acoustic levitator, consisting out of:
  - (a) A wave generator.
  - (b) An electric amplifier.
  - (c) A transducer.
  - (d) A reflector.
2. A laser, focused inside the droplet by a 4X microscope objective.
3. A photographic setup. This setup differed for the 2D and 3D footage:
  - (a) For the normal footage, one high-speed CCD with a 60 mm macro lens was used.
  - (b) For the stereoscopic footage, two CCDS with the same 60 mm lens were used. The cameras were set up perpendicularly with respect to each other. A beam splitter was used to send two different images to the cameras.

#### 3.1.1 Acoustic levitator

As already mentioned in section 3.1, the acoustic levitator consists out of a wave generator, an amplifier, a transducer and a reflector. The wave generator was set to produce a wave of about 27.4 kHz, as the Langevin transducer was observed to produce the strongest sound wave at this frequency. However, the resonance frequency of the transducer changes over time due to heating of the system. Therefore the frequency had to be adjusted (with a maximum of  $\pm 0.1$  kHz) from time to time to maintain sufficient acoustic force.

As can be seen in fig. 3.1, a distance of approximately  $\lambda/2$  is maintained, in accordance with the principles described in section 2.3, to create a strong standing wave; however, this can also be varied a little to adjust the shape of the drop.

#### 3.1.2 Laser setup

The laser pulse used to create the cavitation comes from a Nd:YAG laser (Orion, New wave research, with a 532 nm wavelength and a 6 ns pulse duration). The intensity of the laser pulse can be varied between 0 and 17 mJ to change the energy transferred to the cavitation bubble.

The laser beam is directed towards a 4x microscope objective with prisms. The objective focuses the laser beam, and the focal point is where the cavitation bubble will eventually be located. To check that the beam is focused in the droplet, the laser can be fired at its lowest intensity. The reflection of the laser beam on the droplet will then show its position in the plane perpendicular to the camera's object plane. Further positioning (in the object plane) is done using the camera.

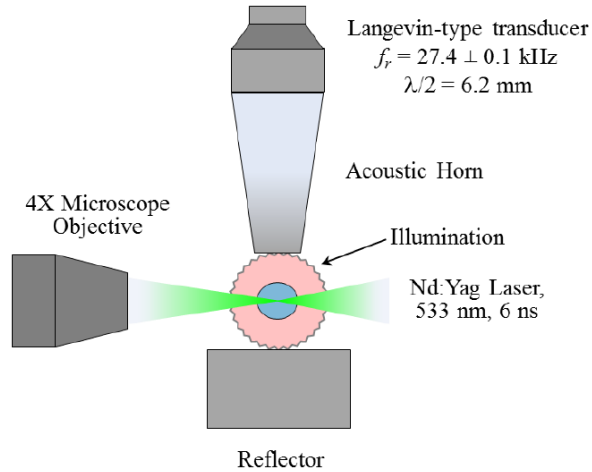


**Figure 3.1:** The setup used in the laser-induced cavitation experiments. Cameras not included in the picture. Source: [18]

### 3.1.3 Camera setup

As cavitation is a very short-lived phenomenon, it is best studied using high-speed imaging. A high-speed camera, a strong illumination source and a trigger to start the camera and the laser pulse are needed for this. The synchronization is done using a pulse delay generator (BNC 575) that triggers both the laser and the camera. The delay between the two can be set arbitrarily. Illumination is provided by a fibre coupled light source that lights a frosted back plane. In some cases, front illumination of the droplet with another fibre coupled light source has been added for increased visibility of the droplet surface perturbations.

Two different camera configurations are used in the experiments. Those experiments that are meant to clarify physical phenomena are recorded with only one high speed camera, and those experiments that aim to visualize the cavitation process in 3D use two cameras instead. How those cameras are set up is explained in the next two subsections.

#### Single camera

All the “normal” experiments have been filmed using a Photron Fastcam SA-X2 mounted with an  $f$  60 mm Nikon lens. The frame rate is 100 000 fps, and a shutter time of  $1/800\,000$  sec is used to prevent excessive motion blur but to still have sufficient illumination. The  $f$ -number is kept at  $f/2.8$ , the highest value possible, to maintain sufficient illumination. However, this does limit the depth of field. The camera is mounted on a  $x$ - $y$ - $z$ -stage, so that it can be positioned relative to the droplet.

A drawback of using a high-speed camera is the maximum resolution. Because all of the data coming from the camera has to be stored in the memory of the camera, the maximum data transfer rate limits the maximum resolution when the frame rate becomes sufficiently high. The images captured with the single camera therefore have a resolution of  $256 \times 256$  pixels.

#### Stereo cameras

To shoot stereoscopic footage one needs, as explained in section 2.4, two cameras. In this research, a Photron Fastcam SA-X2 and a Photron Fastcam SA1.1 are used, both with an  $f$  60 mm Nikon lens. The combinations of frame rate, resolution and shutter time that can be set for the SA1.1 and the SA-X2 differ, and therefore a frame rate of 40 000 fps, a shutter time of  $1/996\,923$  sec and  $1/1\,000\,000$  sec respectively, and a resolution of  $384 \times 320$  pixels are used for the stereoscopic experiments. The aperture is left unchanged at an  $f$ -number of  $f/2.8$  for both cameras in these experiments.

Because the cameras, which shoot macro video, have to be close to the object, and because the cameras are quite bulky, they cannot be set next to each other. This has been solved by using a 50-50 mirror,

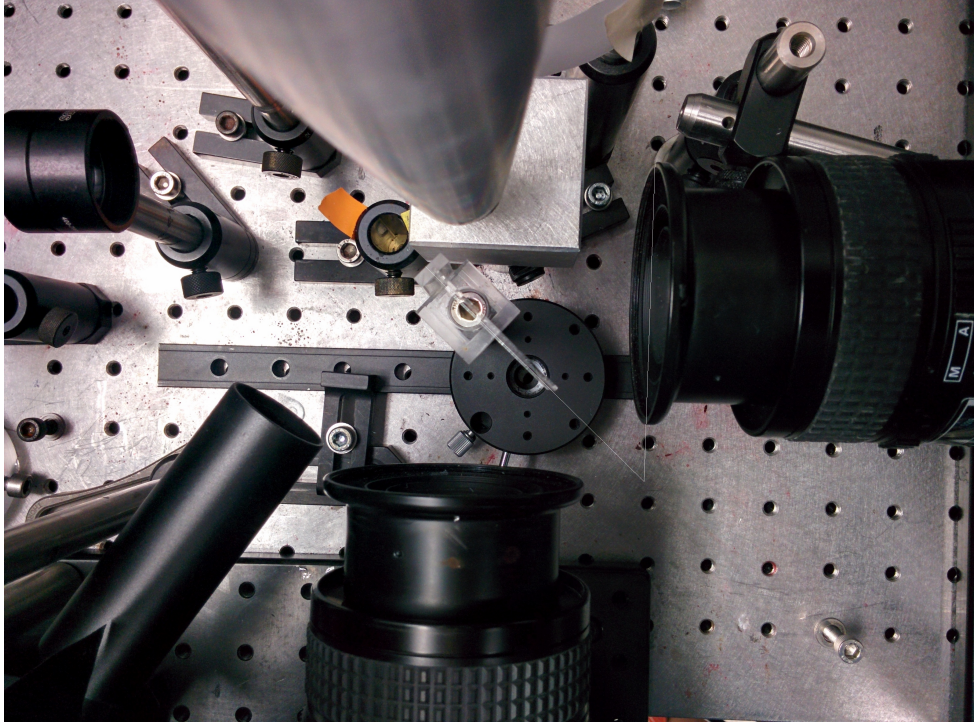


**Figure 3.2:** *The setup for shooting stereoscopic footage. The angle between the mirror and the second camera has been indicated in grey.*

which lets through half of the light hitting it and reflects the other half. Thus, the cameras can be set perpendicular to each other, with one camera receiving the transmitted and one camera receiving the reflected light. The angle of the mirror with the second camera, that records the reflected light, determines the amount depth created in the picture. If the mirror has an angle of exactly  $45^\circ$ , both cameras will produce the same image, but when the angle is de- or increased, the image captured by the second camera will be as if it would be positioned to the left or the right of the other camera respectively. This procedure is applied in the capturing the 3D images for this research, as can be seen in fig. 3.2.

## 3.2 Methods

Once captured, the videos recorded by the high speed camera(s) have to be enhanced for proper viewing. For the normal images, this mainly involves increasing contrast, as the pictures are generally a bit dark due to the short shutter times. For the stereoscopic images, this involves compiling them into a stereoscopic picture as well. These processes are further elaborated in the next sections.

### 3.2.1 Normal images processing

The normal images do not need a lot of processing, as they are preferably viewed “as-is”. However, some of the movies turned out a bit dark, and therefore need a bit of processing. The most convenient adjustment is gamma correction, as this increases the contrast for faint objects while leaving bright objects largely unchanged (for a value of  $\gamma < 1$ ). Image processing is done with ImageJ, which, according to the user guide, uses the following formula for gamma correction:

$$f(p) = \left( \frac{p}{255} \right)^\gamma \times 255 \quad (3.1)$$

Typically, values of  $\gamma$  used for the processing are  $0.4 \leq \gamma \leq 0.6$ . If deemed useful to improve visibility, the contrast and the brightness are adjusted as well.

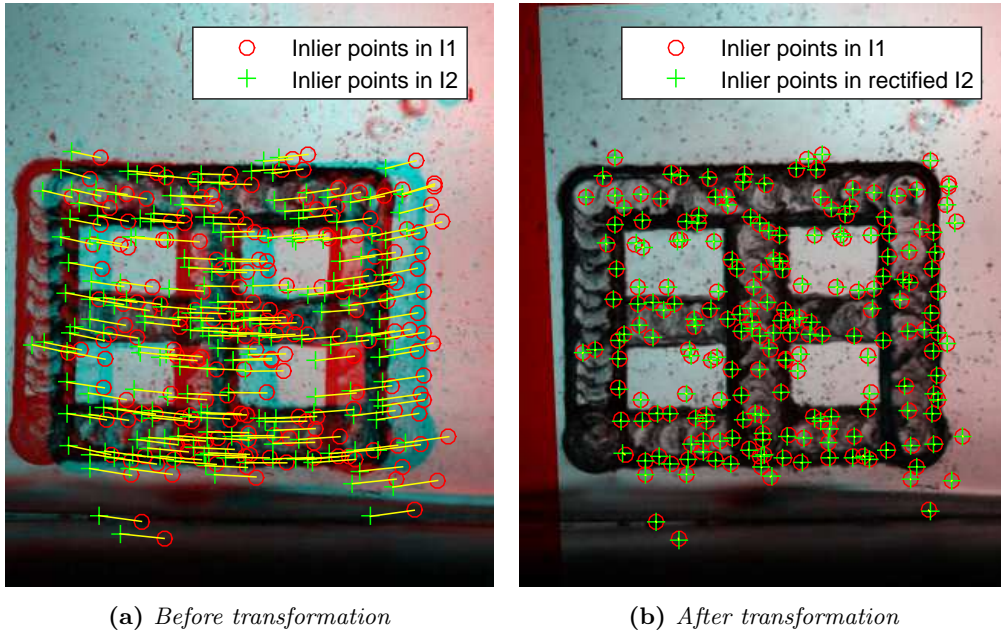


**Figure 3.3:** *The calibration process. Feature recognition is used to find matching points in images 1 and 2, and a transformation matrix is determined that maps the second image into the first. Excessive translation and rotation are thus removed from the picture set. The code used is given in appendix A.*

### 3.2.2 Stereoscopic images processing

Several ways are available to display 3D images and videos, but some of them require special screens or expensive glasses. Therefore, this research uses the anaglyph technique. To view anaglyph images or videos, colour-coded glasses are needed. Our anaglyph videos and images make use of red-cyan colour coding, the most widely used standard.

The principle is fairly simple: the left glass only lets red light pass, whereas the right glass lets blue and green light (the colours that make up cyan) through. Therefore, if the images of the left and right camera are combined into one image with a red and cyan filter applied to the left and right picture respectively, both eyes see something different when looking at the combined image. The brain is able to process this into one image, and the differences between the pictures create a 3D effect.

However, the human brain is not able to process left and right images if they are too different. Especially large translations between the images and rotations cause a lot of trouble, and therefore they should be filtered out. For this purpose, the setup is first calibrated before filming using a 3D structure milled into a transparent piece of plastic. A transformation matrix is determined with MATLAB by comparing the two images, and then applied to the second picture to map it into the first picture. An example of the calibration process is given in fig. 3.3, and the MATLAB code used is given in appendix A.

The transformation matrix determined by the calibration script is saved and used to transform the videos as well. Additionally, both movies are trimmed, so that only the region that is in both videos is included in the final 3D movie. Lastly, the left image is written to the red channel of the (RGB) movie, and the right image to the green and blue channels, thus creating an anaglyph movie. The MATLAB code used to create it is given in appendix B.

## 3.3 Conclusion

In this chapter, both the experimental and recording setup have been outlined, followed by a brief description of the methods used to process the recorded footage. The footage that has been recorded using these setups shows some interesting phenomena, which will be presented in the next chapter.

## 4 Results

In this chapter, the results of the internship are discussed. They are grouped around the same themes that are discussed in chapter 2: bubble-surface interaction, shockwave-surface interaction, acoustic levitator design and stereoscopic imaging.

Unfortunately, not enough (consistent) experiments have been done to be able to draw quantitative conclusions. However, some interesting phenomena can still be observed and described qualitatively using the images of the experiments.

### 4.1 Bubble-surface interaction

As described in chapter 2, the free surface and a cavitation bubble interact if they are close to each other, forming a spike or splash on the free surface close to the cavitation bubble and a counterjet emitted in the opposite direction. Indeed, this was observed in our research as well, as can be seen in the example of fig. 4.1. Indeed we see here a microjet, followed by a broader splash, that is emitted on the side of the droplet close to the bubble, and a counterjet that leaves the droplet on the opposite side. The cavitation bubble is also clearly pushed away from the droplet surface by the accelerated liquid, as predicted by theory. Interestingly, the microjet observed in this example was not observed at all by Obreschkow et al in their experiments [3]. This could be due to the different droplet geometry in their experiment and ours (their droplet is spherical, ours is elliptic), or due to an unseen effect of the laser close to the surface. Interestingly, the splash and the counterjet do not appear always. For low laser intensities, both are not observed at all, and for bubbles which are sufficiently far away from the surface, no microjet or splash can be observed. Apparently the bubble has to be close to the surface to build up sufficient pressure to create a splash.

Another interesting phenomenon caused by cavitation is rupture of the droplet surface. In the example shown in fig. 4.1, the cavitation bubble does not carry sufficient energy to rupture the droplet. However, in certain circumstances it is possible that the bubble partially or completely ruptures the droplet, instead of moving through the liquid. An example of this is seen in fig. 4.2. The cavitation bubble is situated on the left side, and very rapidly grows to more than half of the size of the droplet. The droplet then ruptures on the left side, forming a sheet that accelerates to the right and eventually forms a drop again. A microjet leaving the droplet on the left can also be observed again at the moment of bubble creation. A counterjet is formed as well, but is harder to observe in this case due to acceleration of the ruptured surface surrounding it.

Because the droplet in fig. 4.2 is still rather big (approximately 2 mm), it does not break up completely, even though the laser beam is fairly intense. This is different for smaller droplets, as can be seen in fig. 4.8, which shows 3D footage of the rupture of a small droplet.

### 4.2 Shockwave influence

The influence of the shockwave is again divided into interaction with the droplet surface (the Richtmyer-Meshkov instability) and the effect of secondary cavitation in the droplet. Both are discussed in the next sections.

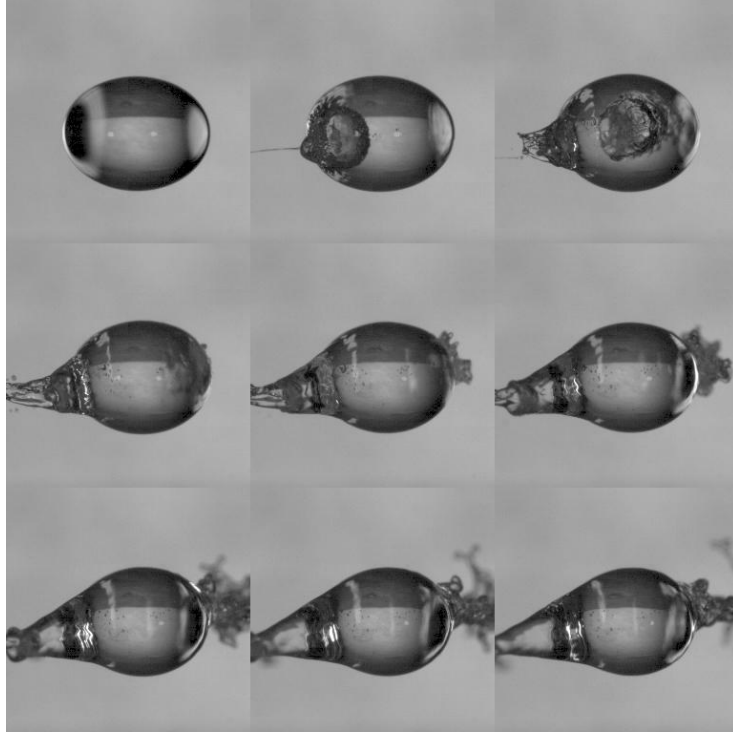


**Figure 4.1:** Image stills of a droplet interacting with a cavitation bubble. The laser is running at 50% of its power, and every tenth frame from frame 1 to 81 is shown in the sequence. The laser impacts in frame 4, so in between the first and second picture shown. Size  $256 \times 256$  pixels. One pixel corresponds to  $20 \mu\text{m}$ .

#### 4.2.1 Richtmyer-Meshkov instability

As described in chapter 2, the interaction between the shockwaves emitted by the creation and collapse of a bubble and the free surface of the droplet is expected to lead to a Richtmyer-Meshkov instability. Because of the surface tension of the droplet surface, this should cause capillary waves that form on the surface.

Indeed, when looking at the available sequences, there seem to be instabilities on the surface that bear some resemblance to capillary waves. This can be seen in e.g. fig. 4.4, where an instability develops on the left side. Tiny bubbles can be seen inside of the droplet before the surface deformation starts, and I suspect that they form the initial surface perturbation: the gas bubbles are pushed out of the drop by the cavitation bubble, deforming the surface. Then the surface, which is rapidly accelerated both due to the bubble pushing it outwards and due to the shockwaves that hit it, deforms rapidly and ejects microjets there where it is deformed. Extra acceleration is seen just after bubble collapse, supporting the theory that a shockwave causes it. Furthermore, ripples spread over the whole droplet from the region with microjets, which supports the theory of capillary waves on the surface. The effect of those waves lasts long after the cavitation bubble is already gone.

Interestingly, the instabilities on the surface also seem to obey the phase inversion as described in chapter 2: perturbations do not start to grow immediately after the initiation of cavitation or after the bubble collapse, but only one or two frames later. This supports the theory that the instabilities can be treated as Richtmyer-Meshkov instabilities.

However, the shock wave does not always result in the emission of multiple jets. The example in fig. 4.5 shows that, in the absence of severe initial perturbations such as the gas bubble cavities in fig. 4.4, the droplet surface will only show harmonic oscillation due to the interaction with the shockwave. This agrees well with the theory for the Richtmyer-Meshkov instability in the presence of surface tension that was presented in chapter 2.

A shock wave can also have other effects than a full surface perturbation. In several cases, the ejection of two jets, one on the top and one on the bottom of the droplet, can be observed shortly after the laser impacts. Interestingly, the points where these jets emerge always lie on a circle which has the centre of

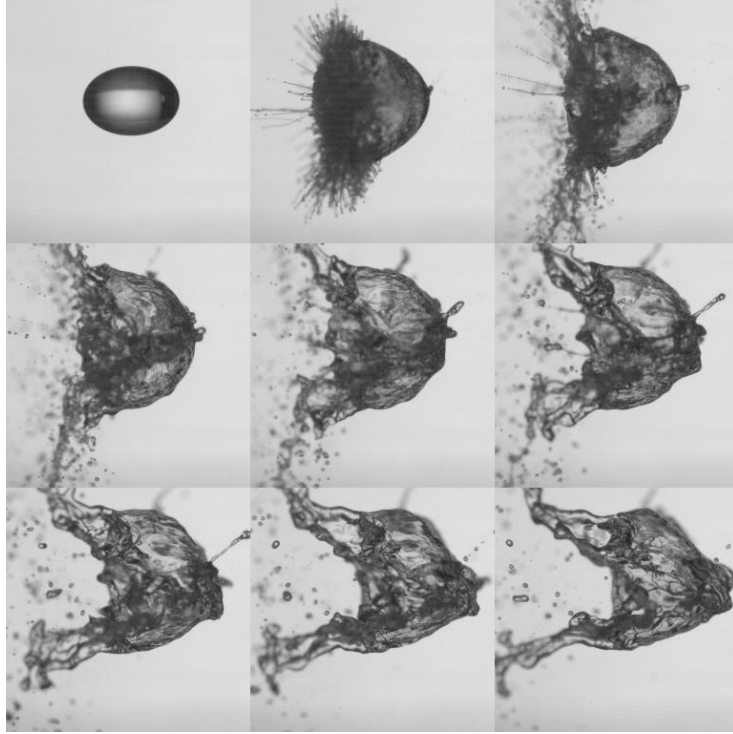


**Figure 4.2:** Image stills of a droplet interacting with a cavitation bubble, forming a sheet. The laser is running at 75% of its power, and every tenth frame from 1 to 81 is shown in the sequence. The laser impacts in frame 4, so in between the first and second picture shown. Picture size:  $256 \times 256$  pixels. One pixel corresponds to  $20 \mu\text{m}$ .

the cavitation bubble as its origin. This is a strong indication that these jets are related to the shockwave emitted at the time of bubble creation, as this shockwave is spherical in shape.

#### 4.2.2 Secondary cavitation

Secondary cavitation is a short-lived phenomenon, but it can be observed in the high-speed movies when paying close attention. A number of our videos show a horizontal and/or vertical ring of small bubbles, created just after the cavitation bubble is created or just after it has collapsed. A clear example is given in fig. 4.6: the top row shows the creation and first expansion of the bubble, and the second row shows stills from just after the first collapse of the bubble. Secondary cavitation can be seen very clearly: in the top middle image, a vertical and horizontal ring are clearly visible, and the left and middle bottom images show a horizontal ring as well. My assumption for the concentration of bubbles in rings is the geometry of the droplet: because the droplet is elliptical rather than spherical, the energy of the shockwaves gets concentrated in these rings by reflections.

### 4.3 Acoustic levitation

As described in section 2.3, the design of the reflector of an acoustic levitator has a big impact on the resulting lifting force. Andrade, Boiuchi and Adamowski have shown in a study that a curved reflector increases the acoustic radiation up to 58 times [15]. The curved radiator design that they have come up with is shown in fig. 4.7. They have tried to find an optimal combination of  $d$ , the distance between transducer and reflector, and  $R$ , the radius of curvature of the curved reflector. Numerical simulation shows that this optimum is found for a distance  $d$  of approximately 19.5 mm and a radius  $R$  of 30 mm.

The acoustic levitation setup in use in the Cavitation Lab at Nanyang Technological University consists out of a flat transducer and a flat reflector, as shown schematically in fig. 2.6. It faces some stability issues: droplets are not properly locked in and therefore show circular movements in the horizontal plane from time to time. Furthermore they often show undesirable shape oscillations due to an unstable acoustic

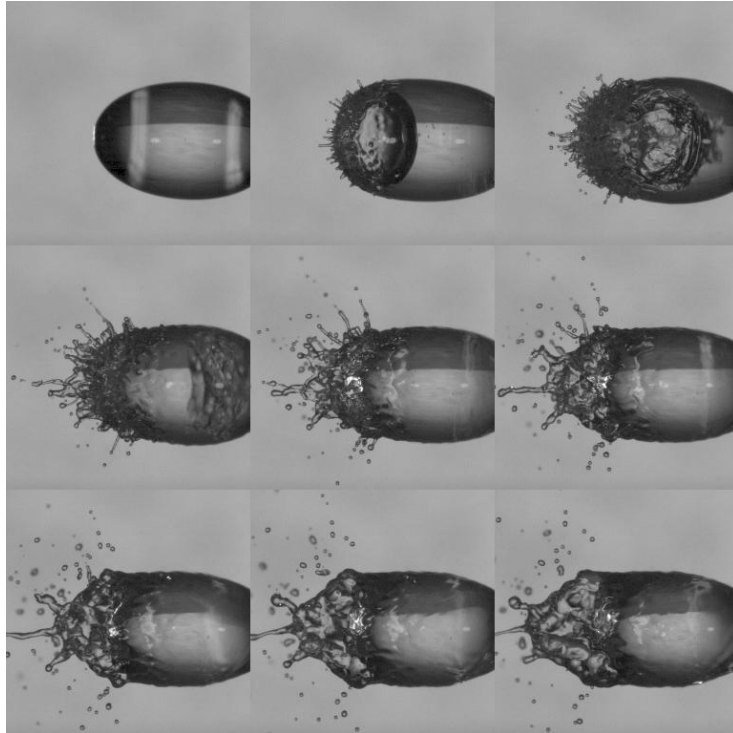


**Figure 4.3:** Image stills of a surface instability developing due to shockwave-surface interaction. The laser is running at 50% of its power, and every tenth frame from 1 to 81 is shown in the sequence. The laser impacts in frame 4, so in between the first and second picture shown. Picture size:  $256 \times 256$  pixels. One pixel corresponds to  $20 \mu\text{m}$ .

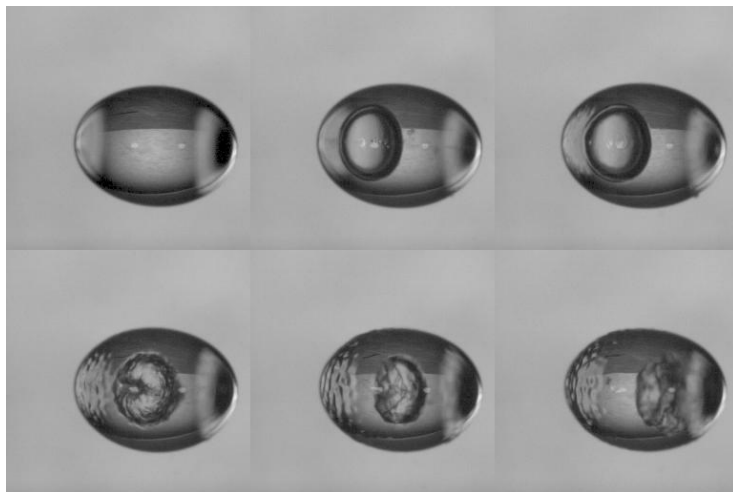


**Figure 4.4:** Image stills of a droplet with an oscillating surface. The laser is running at 53% of its power, and every fifth frame from frame 1 to 26 is shown. The bottom row, with frames from after the first bubble collapse, clearly shows the surface perturbations that have been excited by the collapse shockwave. Picture size:  $256 \times 256$  pixels. One pixel corresponds to  $20 \mu\text{m}$ .

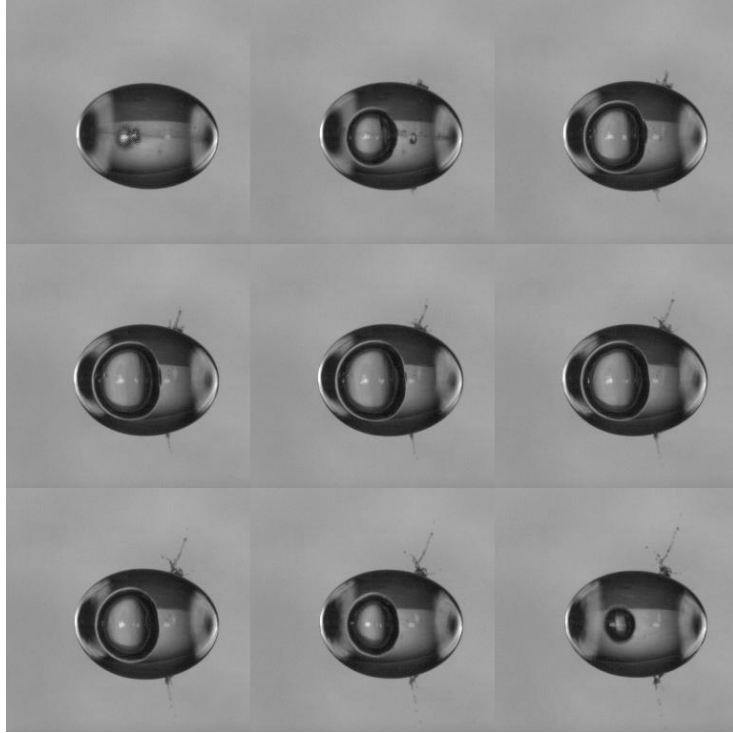


**Figure 4.5:** Image stills of a droplet with two cavitation-induced jets leaving the droplet. The laser is running at 44% of its power, and frames 4 to 12 are shown. The laser impact can be seen clearly in the first image of the sequence. Picture size:  $256 \times 256$  pixels. One pixel corresponds to  $20 \mu\text{m}$ .

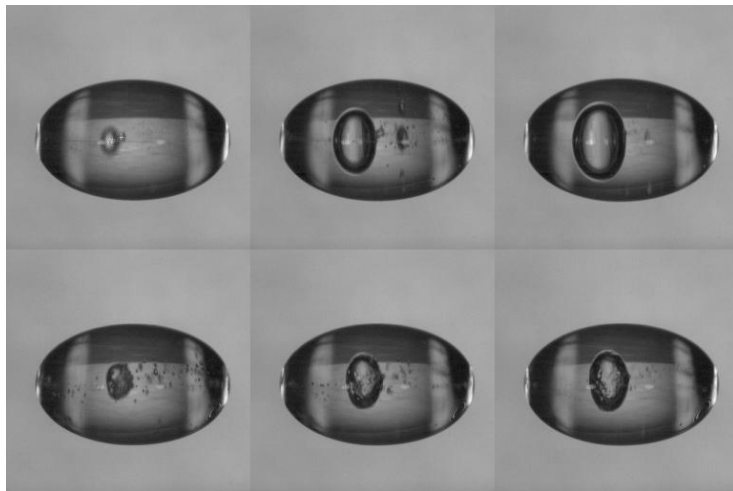


**Figure 4.6:** Image stills of secondary cavitation. The laser is running at 46% of its power. The top row shows frames 4,5 and 6, in which the bubble is expanding, and the bottom row frames 12,13 and 14, in which the bubble collapses and expands again. Picture size:  $256 \times 256$  pixels. One pixel corresponds to  $20 \mu\text{m}$ .

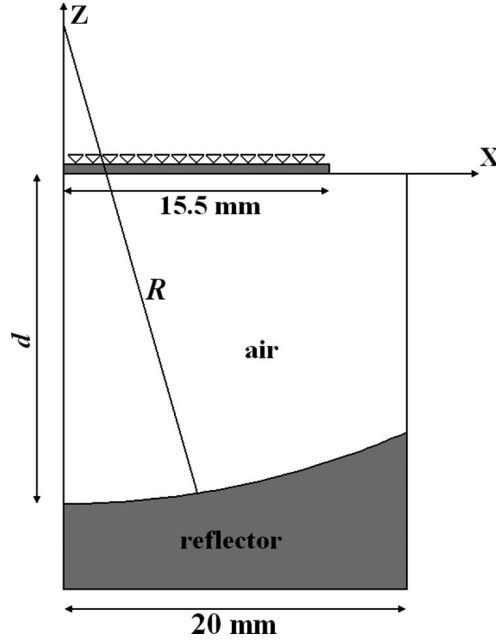


**Figure 4.7:** *The optimised acoustic levitator design proposed by Andrade, Boiuchi and Adamovski [15].*

wave, which sometimes leads to a loss of levitation force. Not only does this make consistent experiments hard, it also makes it impossible to levitate large droplets or liquids with a high density.

A more stable design is therefore of use to the research group, and since the setup used by Andrade et al. looks similar to ours and shows promising results, I decided to try to optimize the setup by using an adaptation of their design. As the design of the transducer could not be altered easily, this was done by scaling their design to ours. The key parameters in this are the radius of the transducer  $R_t$ , the radius of the reflector  $R_r$  and the radius of curvature of the reflector  $R$ . The ratios between those parameters in the optimized design are:

- $\frac{R_t}{R_r} = \frac{15.5}{20} = 0.775$
- $\frac{R_t}{R} = \frac{15.5}{30} \approx 0.517$

The radius of the transducer  $R_t$  of the setup in the cavitation lab is fixed at 11.50 mm, but the design of the new reflector can be chosen freely. The same scaling ratios are therefore applied in a new design made out of aluminium, which has been built by the workshop of the NTU. The parameters used for this design, which have been rounded up to half or whole mms, are:

- $R_r = 15.00 \approx \frac{11.5}{0.775}$
- $R = 22.50 \approx \frac{11.5}{0.517}$
- Height of the reflector  $H = 40$

Unfortunately, the delivery time for parts from the NTU workshop was rather long, and therefore no new experiments could be conducted with the curved reflector. However, short tests indeed showed that the energy input needed to create sufficient acoustic levitation force with the new reflector is drastically lower, and that the levitation points are indeed located where the numerical simulation of Andrade et al. (fig. 2.7) shows them to be. Hopefully this new reflector can therefore be a useful addition to the Cavitation Lab for further experiments.

## 4.4 Stereoscopic images

Lastly, stereoscopic videos have been created during this research. These videos serve as a means of visualisation, not as a method to determine out-of-plane velocity. Therefore, the main goal was to achieve

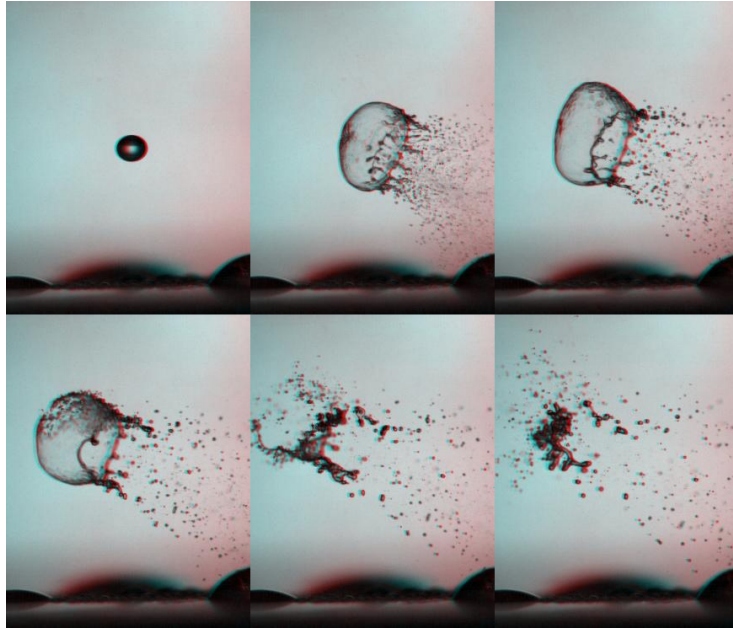


**Figure 4.8:** Image stills of rupturing droplet in 3D; the 3D effect can be seen with anaglyph glasses. The laser is running at 30% of its power. Every fifth frame from frame 1 to 26 is shown. Picture size:  $290 \times 372$  pixels. One pixel corresponds to  $20 \mu\text{m}$ .

an acceptable perception of depth for the human eye with a setup that is as simple as possible. The direct inspiration to do so was a visit by assistant professor Elke Reinhuber from the School of Art, Design and Media to the Cavitation Lab. A lot of her work involves 3D imaging and video, and thus the idea was born.

However, creating an image with acceptable depth proved to be more difficult than expected. The main challenges involved were:

1. The sheer weight of the cameras is so high that it makes the supports that they are leaning on bend. Thus, both cameras film a slightly rotated image, which is slightly hard to correct for.
2. As the cameras are not on the same frame, they are not automatically aligned. This has to be done by eye, which might that small differences might persist after aligning.
3. The angle between the camera and the 50/50 mirror, that splits the light coming from the scene between the two cameras, can only be determined with limited accuracy.
4. The illumination in both pictures varies, so that some post-processing has to be performed to get similar brightness and contrast in the left and right images.
5. The field of focus for the two cameras has to be matched manually, which again means that small differences might persist after matching.
6. The setup is not very robust and thus sensitive to disturbances from the environment.

That being said, some of the footage obtained in the end actually had a reasonable 3D effect. Especially for smaller drops the images obtained in the end were rather good, as they break up into thin films that let through a lot of light and thus show more object features for a better 3D effect. An example is shown in fig. 4.8, where the rupture of a small droplet by cavitation is shown. The 3D effect can be appreciated with anaglyph glasses.

Even though it was hard to obtain good footage with the described 3D setup, it was eventually used to create a movie for the Gallery of Fluid Motion, a yearly contest by the American Physical Society, Division of Fluid Dynamics [19]. And with success: this movie won a 2015 Gallery of Fluid Motion Award. More information on this can be found using the link in the bibliography.

## 5 Conclusions

The goal originally laid out for this research was to look into the influence of a laser-induced cavitation bubble and the cavitation-induced shockwaves on large acoustically levitated droplets. Next to qualitative investigation into these topics, engineering-related work has been carried out as well: the acoustic levitator has been improved, and the existing setup has been modified to be able to produce 3D images.

To begin with, the experimental part of the research has affirmed well-understood phenomena in cavitation bubbles. The observations are in line with existing theory about bubble-surface interactions: the bubble is drawn to and later repulsed by the surface, the bubble can cause formation of a microjet or splash on the surface and a counterjet in the opposite direction, and the bubble decays in several cycles of growth and collapse. Some of the observations also show how a cavitation bubble can rupture the droplet surface if it carries sufficient energy. It is good to see that these well-established relations are observed in our experiments, and my personal learning about the topic has been greatly enlarged by studying them. Furthermore, interesting results were obtained on the field of shockwave-surface interaction. Such an interaction gives rise to what is called the Richtmyer-Meshkov Instability, which is usually studied in practice with a combination of light and heavy gases. However, this research indicates that such an instability occurs at a water/air interface such as the droplet surface as well, and that its behaviour differs a little from standard cases. The behaviour seen is in qualitative agreement with mathematical models for this subject.

On the engineering side, results were achieved both in improving the acoustic levitator by redesigning the reflector and in modifying the setup to create 3D high-speed footage. 3D footage obtained using this setup was later used to create an award-winning movie for the Gallery of Fluid Motion contest by the APS Division of Fluid Dynamics. Especially the last bit is an achievement that I am rather proud of.

For me personally the internship also offered a great learning experience. It was my first encounter with (rather) fundamental research, and that taught me how to approach open questions, which are very different from the closed questions usually encountered during studies. It also was my first longer stay abroad, and a my first stay outside of Europe in general. This was very useful too, as it helps me to understand people from different backgrounds better now. It also has taught me to appreciate the positive sides of our own society a whole lot more.

In short, I think this internship has helped a great deal in my personal development and was a useful contribution to my master programme. I hope that, on top of that, my supervisors deem my work at least a little bit helpful as well.

*Pjotr Kerssens*

# A Calibration procedure

Calibration for the stereo images is performed using MATLAB. The complete code is printed below.

## A.1 MATLAB code

### Stereo movie transformation matrix

This script determines the geometric transform that makes two calibration videos overlap, and the corner-points of the region of overlap of the two. The input arguments are:

- The movie file names 'file1' and 'file2', which are the the left and right image respectively;
- Which frame to use for the estimation of the geometric transform;
- A choice whether (1) or not (any other) intermediate plots and images should be shown;
- The name of the calibration file to be saved.

```
% Only one frame of the movie is used to reduce the computational time. It
% is assumed for this script that both movies have the same number of
% frames.
```

```
clc
clear all
close all
```

```
file1 = 'movies/150603/0306cal4_left.avi'; % Left calibration movie
file2 = 'movies/150603/0306cal4_right.avi'; % Right calibration movie
```

```
rect_frame = 1; % Choose the frame to use for the calculation of the transform
intermediate = 1; % 1 to show intermediate plots, 0 to suppress
calfile = 'calfile.mat'; % The values obtained are stored under this name
```

### Importing the movies

This piece of the code reads the two videos to the Matlab workspace. It is set to load the complete video ('while hasFrame(obj1)'). Replace this expression by ('while k <= X') to load only the first X frames.

```
obj1 = VideoReader(file1);
obj2 = VideoReader(file2);

k = 1;
while hasFrame(obj1)
    mov1(k).cdata = readFrame(obj1);
    mov2(k).cdata = readFrame(obj2);

    k=k+1;
end
```

## Feature detection

In this section the blobs present in the calibration frames are detected. If not enough features are detected, the 'MetricThreshold' can be lowered. Make sure to use a calibration piece for the images that has a lot of contrast to ensure that enough features are detected.

```
I1 = mov1(rect_frame).cdata;
I2 = mov2(rect_frame).cdata;

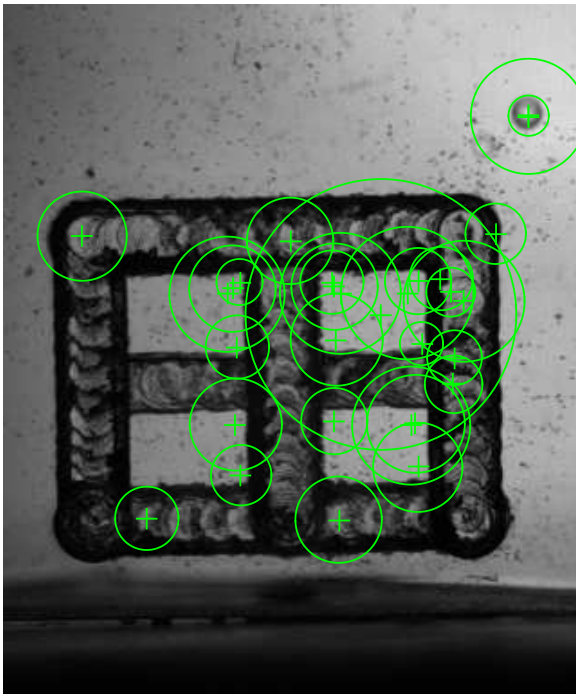
blobs1 = detectSURFFeatures(I1, 'MetricThreshold', 200);
blobs2 = detectSURFFeatures(I2, 'MetricThreshold', 200);

if intermediate == 1
    figure;
    imshow(I1);
    hold on;
    plot(selectStrongest(blobs1, 30));
    title('SURF features in I1');

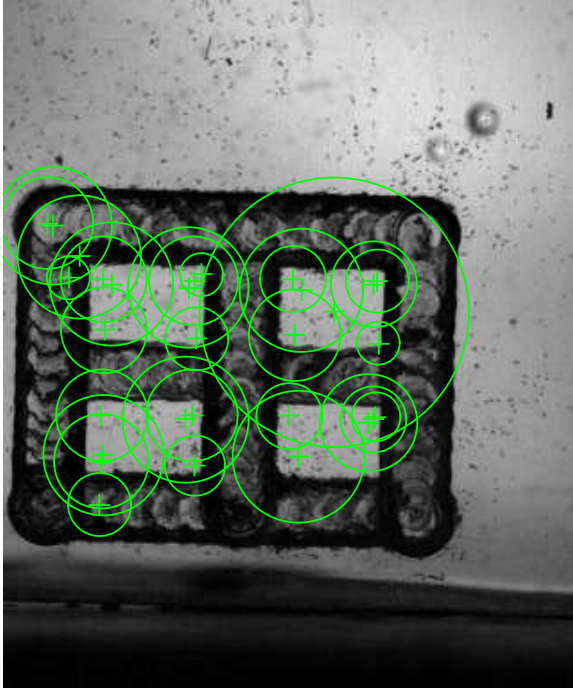
    figure;
    imshow(I2);
    hold on;
    plot(selectStrongest(blobs2, 30));
    title('SURF features in I2');
end

[features1, validBlobs1] = extractFeatures(I1, blobs1);
[features2, validBlobs2] = extractFeatures(I2, blobs2);
```

**SURF features in I1**



## SURF features in I2



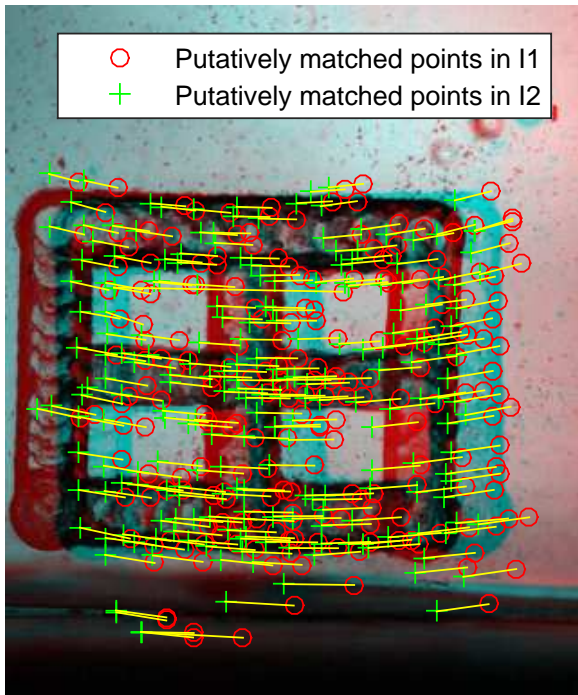
### Matching the features

`matchFeatures` matches features found in both frames. If too many features get rejected in this step, try lowering the 'MatchThreshold', and if too much rubbish comes through, try raising it.

```
indexPairs = matchFeatures(features1, features2, 'Metric', 'SAD', ...
    'MatchThreshold', 5);

matchedPoints1 = validBlobs1(indexPairs(:,1),:);
matchedPoints2 = validBlobs2(indexPairs(:,2),:);

if intermediate == 1
    figure;
    showMatchedFeatures(I1, I2, matchedPoints1, matchedPoints2);
    legend('Putatively matched points in I1', 'Putatively matched points in I2');
end
```



## Calculate transformations

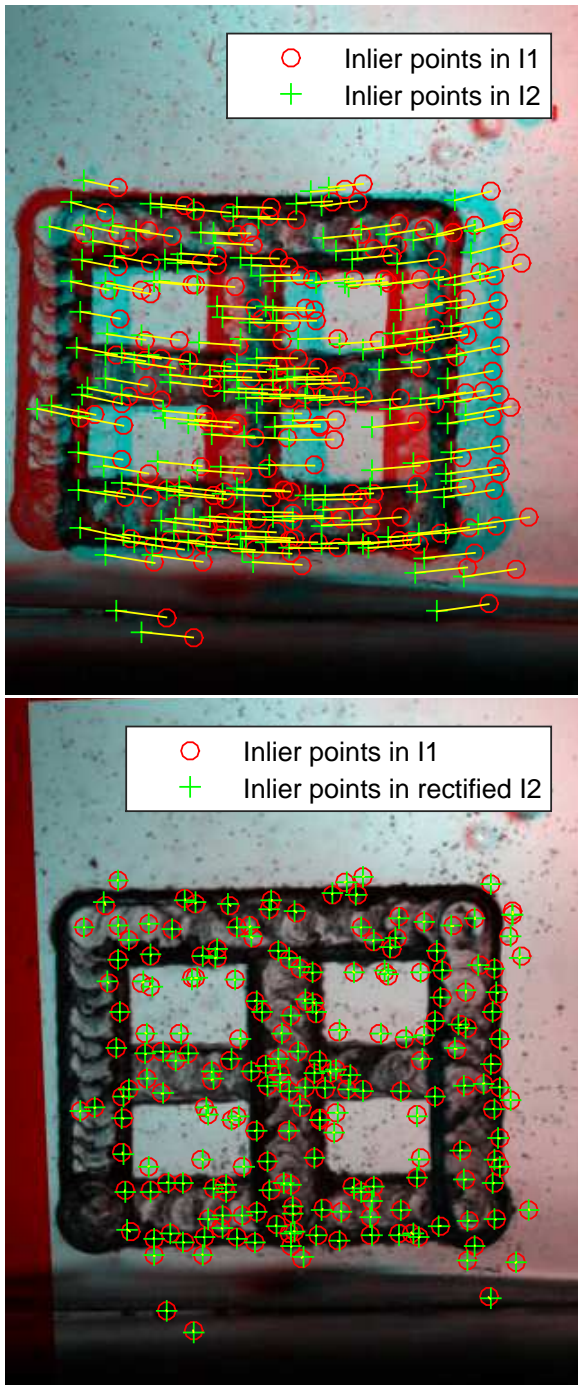
`estimateGeometricTransform` estimates the geometric transform. The inlier points are saved only because they are needed for the intermediate plots.

```
[tform, inlierPoints2, inlierPoints1] = estimateGeometricTransform(...
    matchedPoints2, matchedPoints1, 'similarity');

if intermediate == 1
    figure;
    showMatchedFeatures(I1, I2, inlierPoints1, inlierPoints2);
    legend('Inlier points in I1', 'Inlier points in I2');

    I2Rect = imwarp(I2, tform, 'OutputView', imref2d(size(I2)));

    pts2Rect = transformPointsForward(tform, inlierPoints2.Location);
    figure;
    showMatchedFeatures(I1, I2Rect, inlierPoints1.Location, pts2Rect);
    legend('Inlier points in I1', 'Inlier points in rectified I2');
end
```



## Region of overlap

This last section applies the transform just obtained to the cornerpoints of the second image, thus calculating their location in the coordinates of the first. These values are then used to determine the region of overlap of the two pictures to be able to trim all movies that belong to this calibration.

```

numRows = size(I2,1);
numCols = size(I2,2);
inPts = [1,1; 1,numRows; numCols,numRows; numCols,1];
outPts = transformPointsForward(tform, inPts);
xSort = sort(outPts(:,1));
ySort = sort(outPts(:,2));

```

```

if xSort(2) <= 1
    xLower = 1;
else
    xLower = ceil(xSort(2));
end
if xSort(3) > numCols
    xUpper = numCols;
else
    xUpper = floor(xSort(3));
end
if ySort(2) <= 1
    yLower = 1;
else
    yLower = ceil(ySort(2));
end
if ySort(3) > numRows
    yUpper = numRows;
else
    yUpper = floor(ySort(3));
end

```

### Create a calibration file

The transformation matrix and limits of the region of overlap are now saved in the calibration file 'calfile' specified in the first section. This file can later be used to transform and crop the actual data belonging to this calibration.

```
save(calfile,'tform','xLower','xUpper','yLower','yUpper')
```

# B Anaglyph movie code

All anaglyph movies created in this research have been made with MATLAB. The complete code is printed below.

## B.1 MATLAB code

### Creating an anaglyph stereo movie

This script processes two separate movies into one so-called anaglyph stereo movie. The input arguments are:

- The movie file names 'file1' and 'file2', which are the left and right image respectively;
- The name of the calibration file corresponding to this measurement;
- A choice whether (1) or not (any other) a movie file should be saved;
- The name of the movie to be saved; - The framerate of the movie.

It is assumed that both movies have the same number of frames, and that both are grayscale images.

```
clc
clear all
close all

file1 = 'movies/150603/5_left_enh.avi'; % Left movie
file2 = 'movies/150603/5_right_enh.avi'; % Right movie
calfile = '150603/0306rot4.mat'; % The name of the calibration file

exportfile = 0; % 1 to export the movie, 0 to suppress
movie1 = 'movies/150603/5_3D_enh.avi'; % Name of the movie file to be saved

framerate = 2; % Framerate of the movie
```

### Importing and transforming the movies

In this section all frames of the movies are read, transformed, cropped to the region of overlap and then saved to the workspace. To load only part of the video, replace 'while hasFrame(obj1)' with 'while k <= X', with X representing the desired number of frames.

```
obj1 = VideoReader(file1);
obj2 = VideoReader(file2);
load(calfile)

k = 1;
while hasFrame(obj1)
    I1 = readFrame(obj1);
    I2 = readFrame(obj2);
    I2 = imwarp(I2, tform, 'OutputView', imref2d(size(I2)));
```

```
mov1(k).cdata = I1(yLower:yUpper,xLower:xUpper);  
mov2(k).cdata = I2(yLower:yUpper,xLower:xUpper);
```

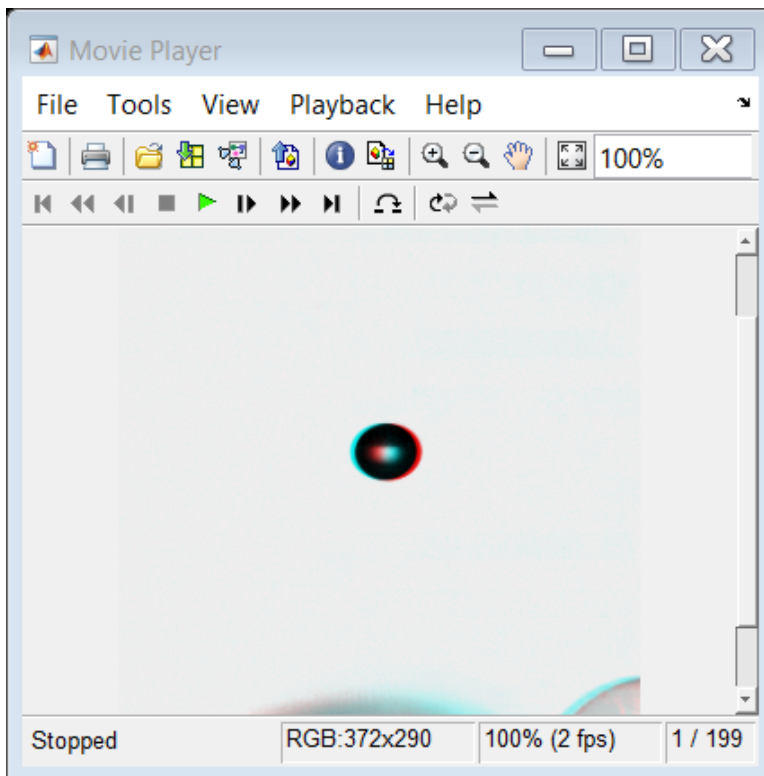
```
k=k+1;
```

```
end
```

## Creating the anaglyph movie

This last part combines the rectified images into an anaglyph movie by writing the left image to the red image layer and the right image to the green and blue layers. The result can be viewed using red-cyan anaglyph glasses.

```
if exportfile == 1  
    writerObj1 = VideoWriter(movie1,'Uncompressed AVI');  
    writerObj1.FrameRate = framerate;  
    open(writerObj1);  
end  
  
for k = 1:length(mov1)  
    mov3D(:,:,k) = cat(3, mov1(k).cdata, mov2(k).cdata, mov2(k).cdata);  
    if exportfile == 1  
        writeVideo(writerObj1,mov3D(:,:,k));  
    end  
end  
  
if exportfile == 1  
    close(writerObj1)  
end  
  
implay(mov3D,framerate)
```



# Glossary

$A$  Atwood number,  $\frac{\rho_A - \rho_L}{\rho_L + \rho_A}$ .

$k$  Wave number.

$P_B$  Internal pressure of the cavitation bubble.

$P_\infty$  Pressure of the surrounding medium.

$R_b$  Radius of the cavitation bubble.

$R_d$  Radius of the levitated droplet.

$S$  Surface tension of the cavitation bubble.

$u$  Velocity.

$U$  Radiation potential.

# List of Greek Symbols

$\eta$  A surface perturbation.

$\nu_L$  Kinematic viscosity of the liquid.

$\rho_A$  Density of the air.

$\rho_L$  Density of the liquid.

# Bibliography

- [1] A. L. Klein, W. Bouwhuis, C. W. Visser, H. Lhuissier, C. Sun, J. H. Snoeijer, E. Villermaux, D. Lohse, and H. Gelderblom, “Drop shaping by laser-pulse impact,” *Phys. Rev. Applied*, vol. 3, p. 044018, Apr 2015.
- [2] V. Y. Banine, K. Koshelev, and G. Swinkels, “Physical processes in euv sources for microlithography,” *Journal of Physics D: Applied Physics*, vol. 44, no. 25, p. 253001, 2011.
- [3] D. Obreschkow, P. Kobel, N. Dorsaz, A. De Bosset, C. Nicollier, and M. Farhat, “Cavitation bubble dynamics inside liquid drops in microgravity,” *Physical review letters*, vol. 97, no. 9, p. 094502, 2006.
- [4] A. Lindinger, J. Hagen, L. D. Socaciu, T. M. Bernhardt, L. Wöste, D. Duft, and T. Leisner, “Time-resolved explosion dynamics of h<sub>2</sub> o droplets induced by femtosecond laser pulses,” *Applied optics*, vol. 43, no. 27, pp. 5263–5269, 2004.
- [5] L. Rayleigh, “Viii. on the pressure developed in a liquid during the collapse of a spherical cavity,” *The London, Edinburgh, and Dublin Philosophical Magazine and Journal of Science*, vol. 34, no. 200, pp. 94–98, 1917.
- [6] M. Plesset, “The dynamics of cavitation bubbles,” *Journal of applied mechanics*, vol. 16, pp. 277–282, 1949.
- [7] W. Lauterborn and T. Kurz, “Physics of bubble oscillations,” *Reports on Progress in Physics*, vol. 73, no. 10, p. 106501, 2010.
- [8] T. Leighton, “Derivation of the rayleigh-pleeset equation in terms of volume,” 2007.
- [9] P. Robinson, J. Blake, T. Kodama, A. Shima, and Y. Tomita, “Interaction of cavitation bubbles with a free surface,” *Journal of applied physics*, vol. 89, no. 12, pp. 8225–8237, 2001.
- [10] R. D. Richtmyer, “Taylor instability in shock acceleration of compressible fluids,” *Communications on Pure and Applied Mathematics*, vol. 13, no. 2, pp. 297–319, 1960.
- [11] E. Meshkov, “Instability of the interface of two gases accelerated by a shock wave,” *Fluid Dynamics*, vol. 4, no. 5, pp. 101–104, 1969.
- [12] M. Brouillette, “The richtmyer-meshkov instability,” *Annual Review of Fluid Mechanics*, vol. 34, no. 1, pp. 445–468, 2002.
- [13] Q. Zhang and M. J. Graham, “A numerical study of richtmyer–meshkov instability driven by cylindrical shocks,” *Physics of Fluids (1994-present)*, vol. 10, no. 4, pp. 974–992, 1998.
- [14] K. O. Mikaelian, “Rayleigh-taylor and richtmyer-meshkov instabilities in multilayer fluids with surface tension,” *Physical Review A*, vol. 42, no. 12, p. 7211, 1990.
- [15] M. A. Andrade, F. Buiocchi, and J. C. Adamowski, “Finite element analysis and optimization of a single-axis acoustic levitator,” *IEEE transactions on ultrasonics, ferroelectrics, and frequency control*, vol. 57, no. 2, pp. 469–479, 2010.
- [16] M. Raffel, C. E. Willert, S. T. Wereley, and J. Kompenhans, “Three-component piv measurements,” in *Particle Image Velocimetry*, pp. 209–239, Springer, 2007.

- [17] F. Zilly, J. Kluger, and P. Kauff, “Production rules for stereo acquisition,” *Proceedings of the IEEE*, vol. 99, no. 4, pp. 590–606, 2011.
- [18] S. R. Gonzalez Avila and C.-D. Ohl, “Cavitation-induced fragmentation of an acoustically-levitated droplet,” in *Journal of Physics: Conference Series*, vol. 656, p. 012017, IOP Publishing, 2015.
- [19] S. R. Gonzalez Avila, P. Kerssens, J. Rapet, and C.-D. Ohl, “Instabilities and fragmentation of drops in 3d.” <http://dx.doi.org/10.1103/APS.DFD.2015.GFM.V0029>, 2015. [Online; accessed 9-August-2016].